

Origin of the hidden energy scale and the f -ratio in geometrically frustrated magnets

Phillip Popp,¹ Arthur P. Ramirez,¹ and Sergey Syzranov¹

¹*Physics Department, University of California, Santa Cruz, California 95064, USA*

(Dated: June 21, 2024)

Sufficiently clean geometrically frustrated (GF) magnets are the largest class of candidate materials that may host quantum spin liquids (QSLs). Some of them have been shown to exhibit spin-glass freezing, potentially precluding QSLs, at the “hidden energy scale”, which is significantly lower than the microscopic energy scale of spin interactions. Here, we investigate the origin of the hidden energy scale and its relationship to the f -ratio, the figure of merit for the degree of frustration in GF magnetic materials. The available experimental and numerical data provide evidence that GF magnets display, universally, two distinct temperature scales in the specific heat, the lowest of which is of the order of the hidden energy scale T^* . We argue that this scale is determined by non-magnetic excitations, similar to spin exchanges in chains of spins. The collective entropy of such excitations matches the entropy of the ground states of the Ising model on the same lattice, which provides a way to verify the proposed scenario in experiment. We further confirm this scenario of the hidden energy scale by numerical simulations of spins on the kagome lattice. As T^* is a property of the clean GF medium, it leads to a constraint on the f -ratio.

Geometrically frustrated (GF) magnets are a promising platform for hosting coveted quantum spin-liquid (QSL) states [1]. The geometry of the lattice combined with antiferromagnetic interactions leads to competing configurations of spins in such materials, obstructing the establishment of magnetic order and possibly giving the magnetic state liquid-like properties.

An important figure characterizing the degree of geometric frustration is the f -ratio [2]

$$f = \theta_W/T_c, \quad (1)$$

where θ_W is the Weiss constant, the characteristic energy scale of interactions between the spins in the material, and T_c is the critical temperature at which the spins order magnetically or undergo spin-glass freezing. On a non-frustrating or weakly frustrating lattice, the critical temperature T_c is determined solely by the interaction strength, and the f -number is of order unity. By contrast, strong geometric frustration prevents magnetic order from establishing and thus significantly lowers the ordering-transition temperature or possibly cancels the transition. Because the f -ratio quantifies a material’s ability to resist long-range order, it has been adopted as a figure-of-merit for the material’s potential to become a QSL.

The temperature T_c in the denominator of Eq. (1) is the temperature at which the magnetic degrees of freedom freeze, either due to the onset of long-range order or spin freezing. As we argue in this paper, the f -ratio may be generalised to include the possibility of freezing of the magnetic degrees of freedom not accompanied by any phase transition at a characteristic temperature T_c . For the materials we discuss in this paper, such a temperature T_c is a property of the clean system.

Indeed, GF magnets have recently been shown [3] to display several surprising, universal trends. Contrary to the common expectation that purifying a material sup-

presses spin-glass freezing, GF magnets exhibit the opposite trend: decreasing the density of vacancy defects, the most common type of disorder in such systems, increases the critical temperature of the spin-glass (SG) transition. For vanishingly low vacancy concentrations, a GF material would undergo a spin-glass transition at a “hidden energy scale” $T^* \lesssim \theta_W/10$, which remains finite despite the disappearance of the SG signal in susceptibility. While it remains difficult to fully eliminate quenched disorder, the purest systems exhibit robust signs of short-range order near T^* in neutron scattering [3–6] and specific heat, the quantity of interest for this work, regardless of the details of quenched disorder.

In this paper, we investigate the origin of the hidden energy scale and its relationship to the f -ratio. We give both experimental and theoretical evidence that the heat capacity $C(T)$ in GF materials exhibits two distinguishable peaks, with the lower-temperature peak located at temperatures of order T^* . When cooled down below that temperature, the material has lost a significant portion of its entropy.

We propose that the hidden energy scale is determined by excitations similar to spin exchanges in chains of spins, whose energy is well separated from the energy of other excitations, similar to spin flips, which give rise to the higher-temperature peak in $C(T)$. We make predictions for the entropy of these excitations, which enables the verification of the proposed scenario of the hidden energy scale in experiments.

The freezing of the magnetic degrees of freedom at temperatures below T^* leads to a constraint on the f -ratio. In the presence of quenched disorder, this freezing may lead to a spin-glass transition.

Evidence for two distinct temperature scales in frustrated magnets. Key to the proposed scenario of the hidden energy scale is our observation, discussed in this paper, that GF magnets universally exhibit two distinct

Lattice	System and references
Kagome	${}^3\text{He}$ on graphite [7, 25] Numerics [10–19], this work
Triangular	NiGa_2S_4 [8] Numerics [20–22]
Hyperkagome	Numerics [23]
Spinel	CuGa_2O_4 [9]

TABLE I. Experimental and numerical evidence for two temperature scales in systems of spins on various geometrically frustrating lattices.

temperature scales in the dependence of $C(T)$ on temperature.

In experiments [7–9] on GF materials, in which the data extend over a large enough temperature range, these two temperature scales manifest themselves in two distinct, well-separated peaks in $C(T)$. This behaviour is mirrored by numerical simulations [10–23] on small clusters of spins on frustrating lattices, exemplified by spins on the kagome lattice, whose heat capacity is shown in Fig. 1. For some of the numerically simulated systems, the lower-temperature peak is less distinguishable from the larger, higher-temperature peak and forms a “shoulder” in its vicinity [19–21]. Because the peaks are readily distinguishable in all experiments in which sufficient data are available, we believe that the merging of the peaks in some of the numerical simulations is a finite-size effect that would go away if simulations of significantly larger systems were possible. In Table I, we summarise available experimental and numerical evidence [24] for the existence of such two temperature scales in GF materials.

Excitations near the hidden energy scale. The higher energy scale in the temperature dependence of the heat capacity C is of order of the Weiss temperature

$$\theta_W \sim ZJ \quad (2)$$

in each material, where Z and J are, respectively, the coordination number of the magnetic sublattice of the material and the characteristic exchange coupling. The scale θ_W can be qualitatively understood as the energy required to flip a spin interacting with Z surrounding spins with the interaction energy J . Hereafter, we focus, for simplicity, on spins-1/2, but the results of our paper hold for arbitrary spins.

To illustrate the origin of the lower energy scale, we

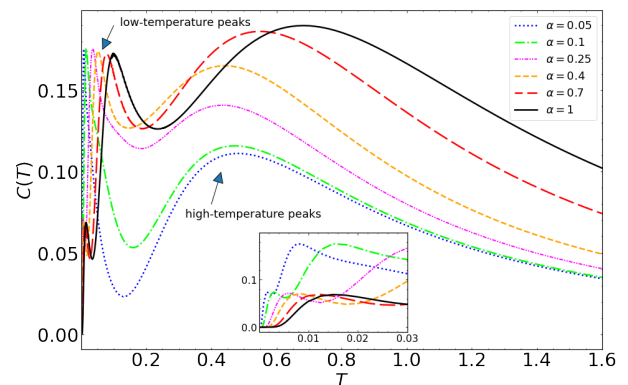


FIG. 1. Heat capacity $C(T)$ (per spin) of the spin-1/2 XXZ model on a cluster of 18 sites on the kagome lattice computed from exact diagonalization with periodic boundary conditions. Different curves correspond to different values of the anisotropy parameter α in the Hamiltonian 3a. The inset shows the behaviour of the heat capacity at very low temperatures, which may display a secondary low-temperature peak. The existence of distinguishable low- and high-temperature peaks in $C(T)$ is in agreement with the results of Refs. [10–16, 18] for the isotropic Heisenberg model ($\alpha = 1$) and of Refs. [18] for the XXZ models. As we clarify in the Supplemental Material [26], the peaks may merge and turn into a plateau for $\alpha \sim 1$ and other boundary conditions.

consider the Hamiltonian

$$\hat{\mathcal{H}} = \hat{\mathcal{H}}_{\text{Ising}} + \hat{\mathcal{H}}_{\text{XY}} + \hat{\mathcal{H}}_{\text{disorder}} + \hat{\mathcal{H}}_{\text{weak}} \quad (3a)$$

$$\hat{\mathcal{H}}_{\text{Ising}} = J \sum_{(ij)} \hat{S}_i^z \hat{S}_j^z \quad (3b)$$

$$\hat{\mathcal{H}}_{\text{XY}} = \alpha J \sum_{(ij)} \left(\hat{S}_i^x \hat{S}_j^x + \hat{S}_i^y \hat{S}_j^y \right) \quad (3c)$$

of spins on a GF lattice, where the part $\hat{\mathcal{H}}_{\text{Ising}} + \hat{\mathcal{H}}_{\text{XY}}$

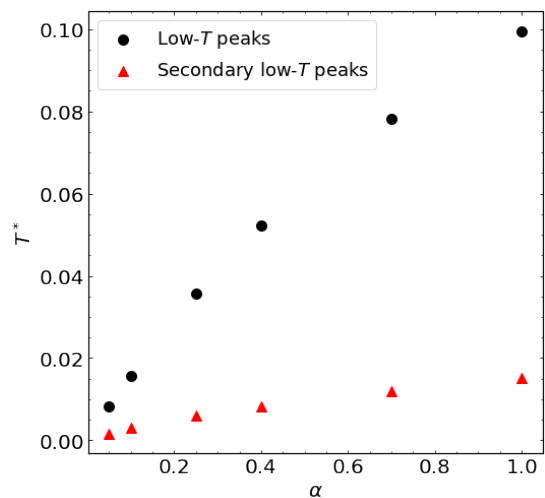


FIG. 2. Temperatures of the low-temperature and secondary low-temperature peaks vs. the anisotropy parameter α .

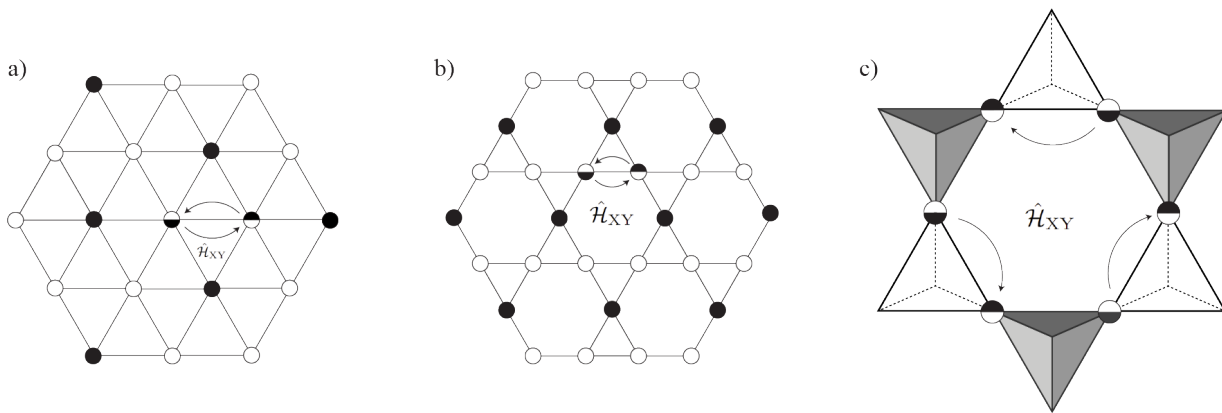


FIG. 3. Illustrations of Ising ground state hybridization via the transverse coupling $\hat{\mathcal{H}}_{XY}$ on the a) triangular, b) kagome, and c) pyrochlore lattices. Each picture shows two Ising ground states which are hybridized by $\hat{\mathcal{H}}_{XY}$. Fully-filled (open) circles indicate spin-up (down) on the corresponding sites, and are the same between the two states. Half-filled circles are read horizontally, with the upper spin orientations applying to one Ising state and the lower orientations to the other.

describes a Heisenberg XXZ model; the summation is carried out over all pairs (ij) of neighbouring spins; J is the coupling strength between the spins' z components; $\hat{\mathcal{H}}_{\text{disorder}}$ is a perturbation created by weak quenched disorder whose exact form is not important for the following arguments; $\hat{\mathcal{H}}_{\text{weak}}$ accounts for weak non-exchange, e.g. dipole-dipole, interactions between spins with characteristic energies significantly smaller than J , and the anisotropy parameter α describes the relative strength of the transverse and longitudinal exchange interactions.

At $\alpha = 0$ (the Ising limit) and $\hat{\mathcal{H}}_{\text{disorder}} = \hat{\mathcal{H}}_{\text{weak}} = 0$, spins on a GF lattice have extensive degeneracy, i.e. degeneracy that scales exponentially with the system size, whereas single spin-flip excitations have a characteristic energy of the order of $\theta_W \sim JZ$.

For small $0 < \alpha \ll 1$ and in the presence of weak disorder and other interactions, the degeneracy of the ground states is lifted, but the energies of respective low-lying excitations remain well separated from the characteristic energies of the excitations of the Ising model. Thus, at small α and weak disorder and other interactions, the model exhibits two types of excitations, adiabatically connected to, respectively, the ground states and the excited states of the Ising model, which gives rise to the two peaks in the heat capacity $C(T)$. We argue below that for most materials, the two peaks remain well separated for $\alpha \sim 1$, which includes the case of the isotropic Heisenberg model.

Indeed, for nonzero α , the ground states of the Ising model become hybridized by the transverse-coupling Hamiltonian $\hat{\mathcal{H}}_{XY}$ given by Eq. (3c). The n -th order transition amplitude between two Ising ground states $|G_1\rangle$ and $|G_2\rangle$ can be estimated as

$$T_{G_1 G_2} \sim \langle G_1 | \hat{\mathcal{H}}_{XY} \left(\hat{H}_{\text{Ising}}^{-1} \hat{\mathcal{H}}_{XY} \right)^{n-1} | G_2 \rangle \quad (4)$$

where \hat{H}_{Ising} is the Ising Hamiltonian $\hat{\mathcal{H}}_{\text{Ising}}$ in the re-

duced space of the excited states of the Ising model. The minimum order n of the processes in which Ising ground states can be hybridized is given by the minimum number Z_1 of pairwise exchange processes of nearest-neighbour antiparallel spins that transform one Ising ground state to another.

Examples of such ‘‘Ising instanton’’ processes are shown in Fig. 3. On the triangular and kagome lattices, there exist Ising states that are distinct from each other by an exchange in only one pair of spins (cf. Figs. 3a and 3b), corresponding to $Z_1 = 1$. For the pyrochlore lattice, the value of Z_1 is 3, corresponding to spin exchange in a loop of 6 spins [27], as shown in Fig. 3c.

The characteristic energies of the excited states, which determine the typical eigenvalues of the operators in Eq. (4), are given by $\theta_W \sim ZJ$, while the matrix elements of the operators $\hat{\mathcal{H}}_{XY}$ are given by $\alpha J/2$. The transition amplitude between the Ising ground states due to Z_1 pairwise spin-exchange processes can, therefore, be estimated as

$$T^* \sim [\alpha J / \theta_W]^{Z_1-1} \alpha J \sim J \alpha^{Z_1} / Z^{Z_1-1}. \quad (5)$$

The quantity (5) describes the characteristic energy splitting between the lowest energy levels of the XXZ model with the Hamiltonian (3a)-(3c) in the limit of weak quenched disorder and weak non-exchange interactions. These states are adiabatically connected to the Ising ground states on the same lattice when the parameter α increases from 0 to a nonzero value. The quantity Z_1 in Eq. (5) is given by the minimum number of pairwise spin-exchange processes that can connect two Ising ground states. The value of Z_1 , like Z , depends on the details of the lattice.

Excitations on the kagome lattice. To further verify the proposed scenario of the lower energy scale, we compute numerically the heat capacity of a cluster of 18 spins on the kagome lattice for various values of α , with the result

shown in Fig. 1. The temperature of the low-temperature peaks, shown in Fig. 2, scales $\propto \alpha$ at small α , which demonstrates that the associated excitations at $\alpha \sim 1$ are adiabatically connected to single spin-exchange processes at $\alpha = 0$ shown in Fig. 3a. We note that the heat capacity $C(T)$ may exhibit an additional, “secondary” peak at low temperatures. Such a feature was also identified for the isotropic Heisenberg model ($\alpha = 1$) in Refs. [15] and [19], where it was suggested to be a finite-size effect.

Constraint on the f -ratio. The scales (2) and (5) in a generic GF material determine the characteristic energies of the excitations that give rise to the two peaks in the behaviour of the heat capacity $C(T)$. As GF lattices typically have coordination numbers in the interval $Z = 4 \dots 6$ and the quantity $Z_1 = 1 \dots 3$, the ratio

$$f = \frac{\theta_W}{T^*} = \left(\frac{Z}{\alpha} \right)^{Z_1} \quad (6)$$

of the higher and lower energy scales is large even when the parameter α is not small, resulting in a separation of the peaks of $C(T)$ in realistic materials.

At temperatures $T \lesssim T^*$, the excitations that give rise to the lower-temperature peak are suppressed, and the magnetic degrees of freedom of the material freeze. The hidden energy scale, thus, constrains the f -ratio in GF magnets. In 3D, in the presence of quenched disorder, this may lead to a spin-glass transition at a temperature $T_c \sim T^*$, which is consistent with the spin-glass freezing observed in GF systems [3] at $T^* \sim 10K$.

The two-peak structure of heat capacity is specific to GF materials. We emphasise that non-GF materials will not, in general, display the two distinct energy scales we have described. Indeed, the ground states of a model that develops long-range magnetic order at low temperatures will not have extensive degeneracy. The excitations that are adiabatically connected to the Ising ground states when α is changed from $\alpha = 0$ to a nonzero value will, therefore, have a vanishing contribution to $C(T)$ per spin and will not lead to the formation of the low-temperature peak.

Lattice	Approximate entropy per site
Kagome	0.50183 ([28, 29])
Triangular	0.323066 ([30–32])
Pyrochlore	0.46 ([33, 34])

TABLE II. Entropy under the lower temperature peak of $C(T)$ for spins-1/2 on various lattices.

Experimental test: entropy related to the “hidden energy scale”. In the experiments [7–9] that have been conducted in a sufficiently large temperature range to

observe both peaks of the heat capacity $C(T)$, the two peaks are well separated from each other. The entropy $S_{\text{low}} = \int_{\text{peak}}^{\text{lower}} \frac{C(T)}{T} dT$ associated with the lower peak is, therefore, a well-defined quantity intrinsic to the pure material. Because the excitations that give rise to that peak are adiabatically connected to the ground states of the Ising model on the same lattice, the associated entropy $S = \int_{\text{peak}}^{\text{lower}} \frac{C(T)}{T} dT$ matches the entropy of the ground states of that Ising model. The value of this entropy also remains unaltered by weak interactions and disorder so long as the peaks of $C(T)$ are well separated.

For common 2D lattices, the values of the respective Ising ground-state entropies can be obtained analytically, while for Ising models on other lattices, the entropy values are known from numerical simulations, as summarised in Table II. Because the values of those (Ising) entropies match the entropies corresponding to the lower peaks in the more complicated, realistic model with the Hamiltonian (3a)-(3c), the value of that entropy can be used as an experimental test of the origin of the hidden energy scale. If the low-temperature behaviour of $C(T)$ also exhibits a secondary low-temperature peak (cf. Fig. 1), the entropy under this secondary peak should be included in the respective entropy of the lower-temperature peak.

Which peak is usually visible in experiments? Often, due to insufficient temperature range, only one of the two peaks is seen in experiments and it is not always clear which peak this is, the low- or the high-temperature one. Our thinking in this paper is focused on data for GF magnets containing 3d elements with θ_W values comparable to or greater than 100K. As a result, there are few $C(T)$ measurements that capture this temperature region and the high-temperature peak (an exception is $NiGa_2S_4$, with $\theta_W = 80K$ [8]). By contrast, in rare-earth frustrated materials, such as $YbMgGaO_4$ ($\theta_W = 4$ K) [35] and $Ce_2Zr_2O_7$ ($\theta_W = 0.6$ K) [36], the experimentally observed peaks in $C(T)$ occur at at 2K and 0.2K respectively. Thus, it is reasonable to associate the peaks observed in those materials with the high-temperature peak in our simulations, while the low-temperature peak likely occurs below 50mK, the practical lower limit of most ultra-low temperature experiments.

Effect of the magnetic field. The low-temperature peak in the behaviour of $C(T)$ will be sensitive or insensitive to the external magnetic field, depending on the lattice and the range of interactions. For some lattices, such as the pyrochlore lattice [37], the “bilayer kagome” lattice of $SrCr_8Ga_4O_{19}$ [38] and the hyperkagome lattice of $Na_4Ir_3O_8$ [39, 40], the Ising ground states have zero magnetization if the exchange interactions between spins are nearest-neighbour. As a result, all the low-energy states of the Heisenberg models that are adiabatically connected to those Ising states have zero magnetizations. For this reason, the low-temperature peak of $C(T)$ in

these materials is independent of the magnetic field, as observed in experiments [38, 39].

By contrast, if the Ising ground states allow for finite magnetizations, exemplified by the triangular and kagome lattices with nearest-neighbour interactions, the low-energy excitations of the corresponding Heisenberg models will, in general, have spins. Such excitations have been reported for the kagome lattice in Refs. [15, 18, 19, 41]. The low-temperature peaks in such materials will be sensitive to the magnetic field.

We also note that in $NiGa_2S_4$, a layered triangular-lattice material, the lower-temperature peak of $C(T)$ is insensitive to the magnetic field [8], which suggests that next-to-nearest-neighbour or interlayer interactions play a significant role in this material, also preventing the long-range order, which would ensue if the interactions were only nearest-neighbour [42–44].

Conclusion. In conclusion, we argue, based on the analysis of available experimental and numerical data, that the temperature dependence of the heat capacity $C(T)$ exhibits two distinct temperature scales. The order of magnitude of the lower scale matches the “hidden energy scale” at which the cleanest of GF magnetic materials undergo the spin-glass-freezing transition and come from excitations similar to pairwise spin exchanges in strings of spins. The entropy associated with the lower-temperature peak matches the entropy of the ground states of the Ising model on the same lattice, which can be used to verify our predictions experimentally. As the value of the hidden energy scale is a property of the clean GF medium, it constrains the f -ratio, characterizing the degree of frustration.

Acknowledgements. We thank V. Elser for useful feedback on the manuscript. Our work has been supported by the NSF grant DMR2218130 and the Committee on Research at the University of California Santa Cruz.

-
- [1] L. Savary and L. Balents, Quantum spin liquids: a review, *Reports on Progress in Physics* **80**, 016502 (2016).
- [2] A. P. Ramirez, Thermodynamic measurements on geometrically frustrated magnets (invited), *Journal of Applied Physics* **70**, 5952 (1991).
- [3] S. V. Syzranov and A. P. Ramirez, Eminent phase in frustrated magnets: a challenge to quantum spin liquids, *Nature Communications* **13**, 2993 (2022).
- [4] C. Broholm, G. Aeppli, G. P. Espinosa, and A. S. Cooper, Antiferromagnetic fluctuations and short-range order in a kagomé lattice, *Phys. Rev. Lett.* **65**, 3173 (1990).
- [5] J. S. Gardner, B. D. Gaulin, S.-H. Lee, C. Broholm, N. P. Raju, and J. E. Greedan, Glassy statics and dynamics in the chemically ordered pyrochlore antiferromagnet $Y_2Mo_2O_7$, *Phys. Rev. Lett.* **83**, 211 (1999).
- [6] C. Stock, S. Jonas, C. Broholm, S. Nakatsuji, Y. Nambu, K. Onuma, Y. Maeno, and J.-H. Chung, Neutron-scattering measurement of incommensurate short-range order in single crystals of the $S = 1$ triangular antiferromagnet $NiGa_2S_4$, *Phys. Rev. Lett.* **105**, 037402 (2010).
- [7] D. S. Greywall and P. A. Busch, Heat capacity of 3He adsorbed on graphite at millikelvin temperatures and near third-layer promotion, *Phys. Rev. Lett.* **62**, 1868 (1989).
- [8] S. Nakatsuji, Y. Nambu, H. Tonomura, O. Sakai, S. Jonas, C. Broholm, H. Tsunetsugu, Y. Qiu, and Y. Maeno, Spin disorder on a triangular lattice, *Science* **309**, 1697 (2005).
- [9] A.P. Ramirez, S-W. Cheong et al., Data for the heat capacity of $CuGa_2O_4$, to be published.
- [10] V. Elser, Nuclear antiferromagnetism in a registered 3He solid, *Phys. Rev. Lett.* **62**, 2405 (1989).
- [11] C. Zeng and V. Elser, Numerical studies of antiferromagnetism on a kagomé net, *Phys. Rev. B* **42**, 8436 (1990).
- [12] N. Elstner and A. P. Young, Spin-1/2 Heisenberg antiferromagnet on the kagome lattice: High-temperature expansion and exact-diagonalization studies, *Phys. Rev. B* **50**, 6871 (1994).
- [13] T. Nakamura and S. Miyashita, Thermodynamic properties of the quantum Heisenberg antiferromagnet on the kagomé lattice, *Phys. Rev. B* **52**, 9174 (1995).
- [14] P. Tomczak and J. Richter, Thermodynamical properties of the Heisenberg antiferromagnet on the kagomé lattice, *Phys. Rev. B* **54**, 9004 (1996).
- [15] P. Sindzingre, G. Misguich, C. Lhuillier, B. Bernu, L. Pierre, C. Waldtmann, and H.-U. Everts, Magneto-thermodynamics of the spin- $\frac{1}{2}$ kagomé antiferromagnet, *Phys. Rev. Lett.* **84**, 2953 (2000).
- [16] G. Misguich and B. Bernu, Specific heat of the $S = \frac{1}{2}$ Heisenberg model on the kagome lattice: High-temperature series expansion analysis, *Phys. Rev. B* **71**, 014417 (2005).
- [17] G. Misguich and P. Sindzingre, Magnetic susceptibility and specific heat of the spin- $\frac{1}{2}$ Heisenberg model on the kagome lattice and experimental data on $ZnCu_3(OH)_6Cl_2$, *The European Physical Journal B* **59**, 305–309 (2007).
- [18] M. Isoda, H. Nakano, and T. Sakai, Specific heat and magnetic susceptibility of Ising-like anisotropic Heisenberg model on kagome lattice, *Journal of the Physical Society of Japan* **80**, 084704 (2011).
- [19] J. Schnack, J. Schulenburg, and J. Richter, Magnetism of the $N = 42$ kagome lattice antiferromagnet, *Phys. Rev. B* **98**, 094423 (2018).
- [20] L. Chen, D.-W. Qu, H. Li, B.-B. Chen, S.-S. Gong, J. von Delft, A. Weichselbaum, and W. Li, Two-temperature scales in the triangular-lattice Heisenberg antiferromagnet, *Phys. Rev. B* **99**, 140404 (2019).
- [21] P. Prelovšek and J. Kokalj, Finite-temperature properties of the extended Heisenberg model on a triangular lattice, *Phys. Rev. B* **98**, 035107 (2018).
- [22] K. Seki and S. Yunoki, Thermodynamic properties of an $S = \frac{1}{2}$ ring-exchange model on the triangular lattice, *Phys. Rev. B* **101**, 235115 (2020).
- [23] T. Hutak, T. Krokhumalskii, O. Derzhko, J. Schnack, and J. Richter, Thermodynamics of the $S = 1/2$ hyperkagome-lattice Heisenberg antiferromagnet, arXiv e-prints, arXiv:2311.08210 (2023), arXiv:2311.08210 [cond-mat.str-el].
- [24] We note the absence of the pyrochlore lattice from the summary of the numerical results in Table I, which we omit because the nature of its heat capacity at low temperatures is not as well-established. For instance,

- in Ref. [45], it is shown that the widely-used finite-temperature Lanczos method yields multiple peaks, while a so-called “entropy method” yields only a single peak.
- [25] K. Ishida, M. Morishita, K. Yawata, and H. Fukuyama, Low temperature heat-capacity anomalies in two-dimensional solid ^3He , *Phys. Rev. Lett.* **79**, 3451 (1997).
- [26] See Supplemental Material at [URL will be inserted by the publisher].
- [27] M. Hermele, M. P. A. Fisher, and L. Balents, Pyrochlore photons: The $U(1)$ spin liquid in a $S = \frac{1}{2}$ three-dimensional frustrated magnet, *Phys. Rev. B* **69**, 064404 (2004).
- [28] K. Kanô and S. Naya, Antiferromagnetism. the kagomé Ising net, *Progress of Theoretical Physics* **10**, 158 (1953).
- [29] R. R. P. Singh and M. Rigol, Thermodynamic properties of kagome antiferromagnets with different perturbations, *Journal of Physics: Conference Series* **145**, 012003 (2009).
- [30] G. H. Wannier, Antiferromagnetism. the triangular Ising net, *Phys. Rev.* **79**, 357 (1950).
- [31] C.-O. Hwang, S.-Y. Kim, D. Kang, and J. M. Kim, Thermodynamic properties of the triangular-lattice Ising antiferromagnet in a uniform magnetic field, *J. Korean Phys. Soc.* **52**, 203 (2008).
- [32] S.-Y. Kim, Ising antiferromagnet on a finite triangular lattice with free boundary conditions, *J. Korean Phys. Soc.* **67**, 1517 (2015).
- [33] A. P. Ramirez, A. Hayashi, R. J. Cava, R. Siddharthan, and B. S. Shastry, Zero-point entropy in ‘spin ice’, *Nature* **399**, 333–335 (1999).
- [34] G. C. Lau, R. S. Freitas, B. G. Ueland, B. D. Muegge, E. L. Duncan, P. Schiffer, and R. J. Cava, Zero-point entropy in stuffed spin-ice, *Nature Physics* **2**, 249–253 (2006).
- [35] J. A. Paddison, M. Daum, Z. Dun, G. Ehlers, Y. Liu, M. B. Stone, H. Zhou, and M. Mourigal, Continuous excitations of the triangular-lattice quantum spin liquid YbMgGaO_4 , *Nature Physics* **13**, 117 (2017).
- [36] B. Gao, T. Chen, D. W. Tam, C.-L. Huang, K. Sasmal, D. T. Adroja, F. Ye, H. Cao, G. Sala, M. B. Stone, *et al.*, Experimental signatures of a three-dimensional quantum spin liquid in effective spin-1/2 $\text{Ce}_2\text{Zr}_2\text{O}_7$ pyrochlore, *Nature Physics* **15**, 1052 (2019).
- [37] S. V. Isakov, K. Gregor, R. Moessner, and S. L. Sondhi, Dipolar spin correlations in classical pyrochlore magnets, *Phys. Rev. Lett.* **93**, 167204 (2004).
- [38] A. P. Ramirez, B. Hessen, and M. Winklemann, Entropy balance and evidence for local spin singlets in a kagomé-like magnet, *Phys. Rev. Lett.* **84**, 2957 (2000).
- [39] Y. Okamoto, M. Nohara, H. Aruga-Katori, and H. Takagi, Spin-liquid state in the $S = 1/2$ hyperkagome antiferromagnet $\text{Na}_4\text{Ir}_3\text{O}_8$, *Phys. Rev. Lett.* **99**, 137207 (2007).
- [40] J. M. Hopkinson, S. V. Isakov, H.-Y. Kee, and Y. B. Kim, Classical antiferromagnet on a hyperkagome lattice, *Phys. Rev. Lett.* **99**, 037201 (2007).
- [41] C. Waldtmann, H.-U. Everts, B. Bernu, C. Lhuillier, P. Sindzingre, P. Lecheminant, and L. Pierre, First excitations of the spin 1/2 Heisenberg antiferromagnet on the kagomé lattice, *The European Physical Journal B* **2**, 501–507 (1998).
- [42] B. Bernu, C. Lhuillier, and L. Pierre, Signature of Néel order in exact spectra of quantum antiferromagnets on finite lattices, *Phys. Rev. Lett.* **69**, 2590 (1992).
- [43] L. Capriotti, A. E. Trumper, and S. Sorella, Long-range Néel order in the triangular Heisenberg model, *Phys. Rev. Lett.* **82**, 3899 (1999).
- [44] S. R. White and A. L. Chernyshev, Néel order in square and triangular lattice Heisenberg models, *Phys. Rev. Lett.* **99**, 127004 (2007).
- [45] O. Derzhko, T. Hutak, T. Krokhnalskii, J. Schnack, and J. Richter, Adapting Planck’s route to investigate the thermodynamics of the spin-half pyrochlore Heisenberg antiferromagnet, *Phys. Rev. B* **101**, 174426 (2020).

Supplemental Material for “Origin of the hidden energy scale and the f -ratio in geometrically frustrated magnets”

In this section, we comment on the dependence of the numerical results for $C(T)$ on the boundary conditions of spin clusters. For the small clusters considered in Refs. [10–19] and in this work, the form of $C(T)$ is sensitive to the boundary conditions. This is exemplified by the two inequivalent 18-site clusters of the kagome lattice shown in Fig. S1. The results we report in Figs. 1 and 2 were obtained using cluster (a), for which we obtain well-separated peaks in the heat capacity $C(T)$ in agreement with Ref. [18]. However, while XXZ Hamiltonians with small values of α on cluster (b) also display two well-separated peaks in $C(T)$, for larger values of α , up through the isotropic Heisenberg case ($\alpha = 1$), the high-temperature peak merges with the low-temperature one, forming a plateau rather than a distinct peak. These behaviours are shown in Fig. S2.

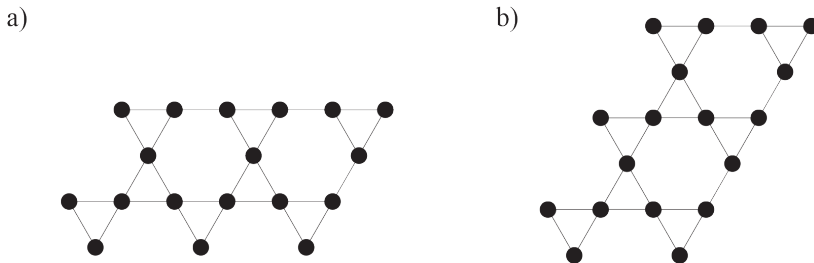


FIG. S1. Two inequivalent 18-site clusters on the kagome lattice. With periodic boundary conditions, cluster (a) has a threefold translation symmetry along the horizontal, while cluster (b) has a threefold translation symmetry along 60° from the horizontal.

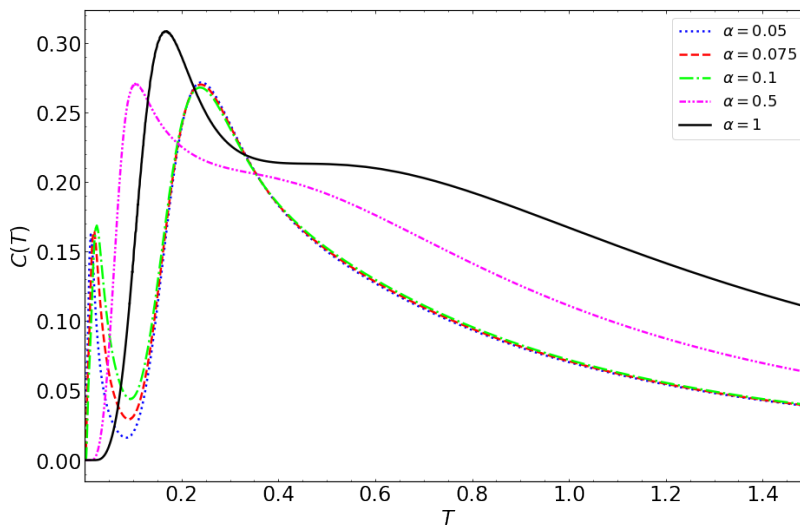


FIG. S2. Heat capacity $C(T)$ (per spin) of the spin-1/2 XXZ model on cluster (b) of Fig. S1. For large values of α , there are not two well-separated peaks, in contrast to heat capacities on cluster (a) and in Ref. [18].

While small spin clusters on the kagome lattice may not display good separation of the peaks in the behaviour of $C(T)$, the two peaks are rather distinct in the available experiments [7, 9, 25] on GF materials, which suggests that the separation improves in the limit of large system sizes, which are currently inaccessible for numerical methods. A more thorough understanding of the effects of boundary conditions and system size on the spectra and thermodynamic properties of kagome clusters awaits future study.